




LUND
UNIVERSITY

Master of science thesis



Absorbed dose distributions in the vicinity of high-density materials in head and neck radiotherapy: A quantitative comparison between measurements, Monte Carlo simulations and treatment planning system

Ulf Bjelkengren

Supervisors:

Sven Bäck, PhD

Lena Wittgren, MSc

Göran Bjelkengren, MD

The work has been performed at
Department of Radiation Physics
Malmö University Hospital

Medical Radiation Physics
Clinical Sciences, Lund
Lund University, 2007

Contents

CONTENTS	3
1. INTRODUCTION	5
2. THEORY	6
2.1 Radiation treatment	6
2.2 Side effects	7
Mucositis	7
Secondary infections.....	8
Xerostomia	8
Radiation caries.....	8
Osteoradionecrosis (ORN)	8
2.3 Treatment planning	9
Treatment planning system	9
Pencil Beam absorbed dose calculation	11
Collapsed Cone absorbed dose calculation.....	12
2.4 Implementation of X-Ray Computed Tomography in the TPS	13
2.5 Monte Carlo Simulations.....	14
3. MATERIALS AND METHODS	15
3.1 The phantom.....	15
3.2 Beam geometry and measurement set up	16
Beam geometry	16
TLD	16
Monte Carlo Simulations	17
Ionization chamber	17
The computer-generated phantom	17
Linear accelerator	18
Treatment planning system	18
CT-scanners.....	18
3.5 Dental materials	19
Gold	19
Porcelain.....	19
Composite.....	19
Titanium	19
4. RESULTS AND DISCUSSION	20
4.1 Evaluation of measurement method and uncertainties	20
4.2 Comparison between the computer-generated phantom, ion-chamber measurements and CT-scanner in water	21
4.3 Evaluation of depth dose curve for gold alloy	22
4.4 Difference between the pencil beam and collapsed cone calculation algorithm.	23
4.5 Evaluation of Hounsfield number implementation in the TPS	24
4.6 Comparison between CT-scanned phantom and computer-generated phantom for porcelain	25
4.7 Comparison between two CT-scanners	26
5. GENERAL DISCUSSION.....	27
6. CONCLUSIONS	28
7. ACKNOWLEDGEMENTS.....	28
<i>APPENDIX 1: DEPTH DOSE CURVES OF DENTAL MATERIALS</i>	29
REFERENCES	33

1. Introduction

In the year 2004, some 50.000 new cases of cancer were diagnosed in Sweden, 2.2 % of these were cancers of the head and neck [1]. The same year the population in Sweden was around nine million people and 100.000 children were born. The total number of deaths in Sweden in 2004 was 90.000 people. The mortality from cancer in 2003 was around 20.000 persons [1].

In the Swedish statistics head and neck cancer diagnoses are divided into cancers of the lip, tongue, salivary glands, floor of mouth, unspecified parts of the mouth, mesopharynx, nasopharynx, hypopharynx, unspecified pharynx, nose, the para-nasal sinus and larynx [1].

When irradiating patients in the head and neck area one must be careful and observant on various side effects. Typical side effects associated with head and neck cancer are mucositis, skin reactions and secondary infections. These are acute, which mean that they occur during and shortly after treatment. Late side effects are xerostomia and caries secondary to the xerostomia. Another, very serious late side effect is osteoradionecrosis (ORN). This deterioration of bone may be very severe and cause pronounced problems for the patient.

Since most of the acutely occurring side effects are temporary the main concern is to prevent xerostomia and osteoradionecrosis. This can be done in different ways that will be described in more detail later.

All side effects are very closely related to the administered absorbed dose and the size of the irradiated volume [2] although late effects are more related to the absorbed dose per fraction [3]. It is thought to be of importance that as many of the patient's teeth as possible are being preserved before and after treatment [4]. Only the most damaged teeth are to be extracted prior to treatment. Because of this approach some of the teeth left might have different types of tooth fillings. These tooth fillings are often made of materials with quite high density compared to other tissues in the oral area [5]. These materials will perturb the calculated dose distributions due to the high density of the different materials compared to the density of the surrounding tissue. A study very recently published, shows that the effect of high-energy photon beams on high-density materials in the head and neck region is of clinical relevance [6]. Another previously published study has shown that metallic implants affect the absorbed dose distributions around hip prostheses and also that the error depends on what calculation algorithm is being used to obtain the absorbed dose distributions [7]. The authors found that there was a discrepancy of 4,1 to 11,7% compared to a Monte-Carlo-simulated dose distribution.

Thus there are several implications that prove that there are discrepancies between the TPS and the actual dose distributions. The isodose lines that represents the dose distributions calculated by the treatment planning system (TPS) does not appear to give homogeneous dose distributions (figure 1.1:1). Another implication is the large image artifacts in the CT-images (figure 1.1:1) that are used as both image material and attenuation material for the dose calculation. These implications are not the only ones but these are enough to make more detailed studies of the effects worthwhile.

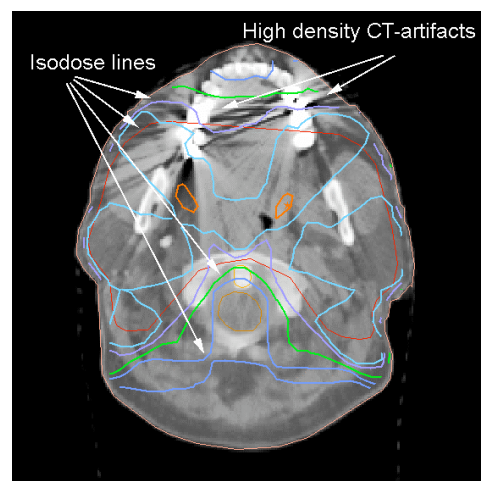


Figure 1.1:1 Example of Isodose-lines and CT-artifacts associated with treatment planning of head and neck cancers. The isodose lines represent the TPS calculated dose distribution

The aim of this study is therefore to quantify the effects that dental materials will have on the calculated dose distributions from the treatment planning system. To be able to quantify this, measurements will be compared with the absorbed dose distributions calculated by a commercial TPS. These calculations will be done on actual CT-data as well as on computer generated phantoms. Further, to support the evaluation of the TPS, the measurements will also be compared with reference dose distributions. These reference dose distributions will be obtained using Monte Carlo simulations

2. Theory

2.1 Radiation treatment

Radiotherapy may be used as the only method or in combination with surgery and/or chemotherapy to treat many head and neck cancers. For cancer of the lips radiotherapy is used in 22% of the cases while it for cancer of the nasopharynx and larynx is used in 100% of the cases [8]. There are two different types of radiotherapy associated with head and neck cancers, external radiotherapy and brachytherapy. In the latter case a probe with a radioactive material (^{192}Ir) will be placed very close to the tumor. In this study only external radiotherapy will be discussed.

Normal tissues show better ability to repair sub-lethal DNA damage than tumor tissue [3]. Because of this, radiotherapy is given as a fractionated treatment. The conventional fractionation scheme for a head and neck cancer is 2 Gy once a day, five days a week leading up a total absorbed dose of 66-70 Gy. In the cases where radiotherapy is given after surgery the total absorbed dose given is 50-60 Gy. This is if complete resection is achieved, if not a boost can be given to incompletely resected areasso that the total absorbed dose reaches 68 Gy [9].

The use of a fractionation scheme also gives another advantage, namely that the fractionation allows for a re-oxygenation of hypoxic tumor tissue [3]. Since oxygenation is crucial for a radiobiological effect on tumor tissue the re-oxygenation is vital to the success of the treatment.

Today, the most common way to give radiation treatment is to use a medical linear accelerator (LINAC). A medical linear accelerator as well as a conventional x-ray tube delivers a poly energetic beam. The difference between the LINAC and the conventional x-ray tube lies in the acceleration of the electrons. In a conventional x-ray tube the electrons are accelerated over a potential of about 120 kV. In this study the LINAC accelerates the electrons over a potential equivalent to 6 MV. To achieve this, the electrons are accelerated on a microwave traversing in a waveguide inside the LINAC before they are collided with a tungsten target to produce bremsstrahlung photons [10].

To achieve local tumor control, the difference between the *tumor control probability (TCP)* and the *normal tissue complication probability (NTCP)* must be as large as possible. This is achieved as mentioned above by a fractionation of the total absorbed dose, and a high precision when delivering the beam. To obtain accuracy in the positioning of the patient prior to treatment, fixations can be used [11]. Typical fixations associated with radiotherapy of head and neck cancers are face-masks and bite-blocks [12]. Typical uncertainties associated with face-masks are standard deviations of 1-5 mm and for bite-blocks 2.7-3.1 mm [12]. If good accuracy is obtained the set-up margins can be decreased.

For a representation of different volumes an international commission (ICRU) has

published a convention that defines volumes of radiological importance [13].

The gross tumor volume (GTV) is the palpable or visible part of the tumor. To assure that no microscopic tumor cell colonies are left outside this volume, margins are added. This yields the clinical target volume (CTV). Because of patient movements, organ movements, set-up uncertainties and variation in accelerator output another marginal is added to the CTV to yield the planning target volume (PTV). Because of these margins the patient can suffer from unwanted side effects. The most sensitive areas in head and neck radiotherapy (Organs At Risk) are the spinal cord, the eyes, mucosa and the parotid glands. If the margins are decreased the dose to the organs at risk (OAR) are decreased and the side effects can be reduced.

For a graphical representation of the calculated distribution of the absorbed dose, a *dose volume histogram (DVH)* is used. A DVH is a simple method to present large 3D-data in a simple diagram. The main purpose of a DVH is to show how much of an anatomical structure, target volume or an OAR that receives a specific amount of absorbed dose (Figure 2.1:1).

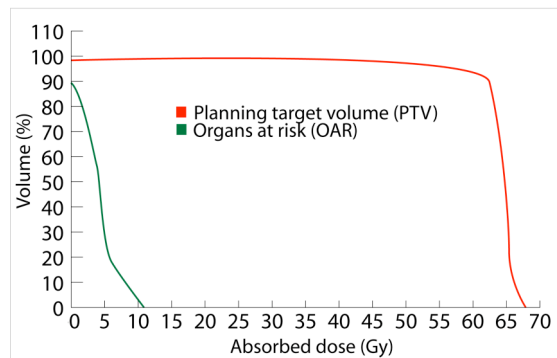


Figure 2.1:1

Example of a DVH with two volumes represented, PTV and OAR

2.2 Side effects

In preparation for this study, literature associated with head and neck cancers has been studied in order to obtain a more detailed insight of the different side effects and potential problems associated with radiotherapy of the head and neck.

Mucositis

The damage to the oral mucosa is strongly dependant on the absorbed dose and the size of the irradiated volume. The fractionation scheme is also a contributing factor to the mucosal reactions. When a fractionation scheme of 2 Gy per day is used, mucosal erythema occurs within one week [14]. The acute mucosal changes are due to mitotic cell death of the epithelial cells, since the cell cycles of the basal keratinocytes is about four days [2]. It is worth mentioning that mucositis is a very individual side effect with a great variety in intensity and duration.

Mucositis begins with a reddening of the oral mucosa. This erythema is due to the previously mentioned thinning of the epithelium and vascular dilation. Inflammation and oedema of the sub mucosa are also contributing factors to this hyperemic state of the mucosa. When the treatment is continued, this hyperemic mucosa becomes ulcerated and covered with a fibrinous exudate [14]. This state is very painful for the patient. Food intake and even speech can be difficult. In some cases even tube feeding can be necessary. The mucositis persists for a couple of weeks after completion of the irradiation. Most of the patients show a complete resolution of mucositis after this time.

Secondary infections

The most common infection associated with radiotherapy is *candidiasis*. Many patients become intra-orally colonized with candida cultures during or shortly after treatment [2]. This colonization is much due to the changes in the antimicrobial defense in the oral cavity. Much of the antimicrobial defense is in the saliva. When the patient is treated, very often the salivary glands are in the irradiated volume. This leads to an alteration and a reduction of the saliva, thus xerostomia is a contributing factor to fungal colonization. It is also thought that mucositis is aggravated by fungal infections [2]. Secondary bacterial infections can also occur due to bacterial overgrowth since the defense mechanisms have been reduced.

Xerostomia

Xerostomia is not like mucositis a transient side effect. Xerostomia is a consequence due to irradiation of the salivary glands, which leads to a decrease in the salivary flow. The major salivary glands accounts for 70-80 % of the salivary flow [14] and consist of the parotid glands, submandibular and sublingual glands. The degree of xerostomia is as for all side effects dependent on the given dose and on the irradiated volume as well as absorbed dose per fraction.

The salivary gland cells are highly differentiated with long cell cycles. This should mean that salivary glands are somewhat radio resistant but this is not the case [2]. Already after two weeks of a 2 Gy per day scheme the flow rates are down by 80% of its initial flow [2]. If this is a reaction on salivary gland tissue caused by the radiation or secondary to injury of the fine vascular structure is not clear [2]. Permanent hyposalivation due to radiation typically occurs when doses reach 40 Gy and above [14]. A decrease in salivary flow and alteration of the saliva opens up for all kind of infections like previously mentioned candidiasis. Taste loss is also a side effect of hyposalivation. The saliva acts as stimuli for the taste buds.

The best way to prevent hyposalivation is to make sure that as little as possible of the salivary glands are within the irradiated volume. This can be done either by shielding the glands with lead blocks, multi leaf collimators etc. or to surgically move the glands [15]. There is no commercially available product to substitute saliva although some products try to mimic its lubricating capabilities. Persons suffering of xerostomia are recommended to always carry a bottle of water to moisten the oral mucosa. Salivary flow from the parotid glands can be stimulated with fruits containing citric acid if the glands are not completely destroyed [14]. Though one must be careful on the effects of the acid on the teeth.

Radiation caries

Radiation caries is a very destructive form of caries. In severe cases radiation caries can destroy a healthy dentation within one year [2]. Radiation caries is an effect due to the increase of cariogenic microorganisms. The increase of these microorganisms is due to changes in the saliva when the salivary glands are irradiated.

Osteoradionecrosis (ORN)

There are two kinds of osteoradionecrosis, spontaneous and non-spontaneous induced osteoradionecrosis. Spontaneous ORN accounts for about 35 % of the osteoradionecrosis. This type of ORN is related to the age of the patient and high radiation dose (above 65 Gy).

Another contributing factor is the volume of the mandible located in the radiation field [2]. Non-spontaneous ORN is almost always associated with trauma. In 88 % of the cases this trauma is caused by tooth extractions [14] but the source of trauma might be anything from irritation of ill-fitting dentures to sharp and hard food particles and sharp bony ridges [2]. Osteoradionecrosis is considered as an infectious process with trauma serving as entry port for bacteria into the underlying bone [2]. Most cases of ORN occur in the mandible because the density is high and vascularization is low. The condition is characterized by necrotic tissues and bone that fails to heal spontaneously [16].

To prevent osteoradionecrosis, damaged teeth are extracted prior to radiotherapy. This is done to prevent any infection due to infected roots, bony spicules or any other dental pathology [17]. The extractions should be done at least two weeks before radiotherapy to leave room for the healing processes [15]. Osteoradionecrosis is a lifelong concern and the dentist must be informed of this and take extra care of the patient. For example, specialists in dental surgery should always do teeth extractions after radiotherapy. The patients must also take extra care in their oral hygiene. Poor oral hygiene and the use of tobacco and alcohol are known factors that may lead to a rapid onset of osteoradionecrosis [17].

2.3 Treatment planning

A treatment planning system is used to calculate absorbed dose calculations for the radiation treatment. These calculations are often very complex which makes it difficult to explain how they are implemented in the TPS without a deeper insight in the physics and mathematics surrounding them. The descriptions of how the treatment planning system calculates the absorbed dose is described in below.

Treatment planning system

A modern treatment planning system uses an energy fluence based dose formalism [18]. This means that the TPS calculates the absorbed dose to the patient from the amount of radiant energy per area traversing a cross section of the beam from the accelerator. Since the ion chambers in the LINAC head measures the same quantity to control the output of the accelerator this means that there is a direct physical approach between the internal calculations in the TPS, the beam delivery and dose monitoring system in the accelerator. The energy fluence based dose formalism also allows for complex fields such as irregular and asymmetric fields, dynamic wedges, multi leaf collimators etc. [18].

The energy fluence distribution from the clinical beam can be denoted by $\psi_{tot}(x, y)$. This is defined as the amount of radiant energy per area, ΔA at position (x, y) traversing a plane perpendicular to the beam, i.e.

$$\psi_{tot}(x, y) = \sum_i \frac{N_{E_i}(x, y) \cdot E_i}{\Delta A} \quad (1)$$

In this approach it is assumed that the energy fluence is given at a reference distance, z_0 , in this case at the isocenter distance. The term $N_{E_i}(x, y)$ is the number of photons with energy E_i traversing the plane (x, y) .

Since a clinical beam contains scatter from various irradiated sources in the LINAC head, one must add a factor to the total energy fluence to correctly describe such scatter.

$$\psi_{tot}(A; x, y) = \psi_{dir}(x, y) \cdot \eta(x, y) + \psi_{cont}(A; x, y) \quad (2)$$

The term $\psi_{dir}(x, y)$ describes the direct incident, non-scattered energy fluence, $\eta(x, y)$ is an eventual modulation of the beam. $\psi_{cont}(A; x, y)$ is the energy fluence from contaminating scattered photons in the machine treatment head. A is a formal variable that represents the aperture. Since the contaminating photons originate from several different parts of the treatment head it is often of interest to divide this part into several different components. These consist of the scattered part of the energy fluence from the flattening filter and the primary collimator, $\psi_f(A; x, y)$, other collimators and block edges, $\psi_c(A; x, y)$ and other auxiliary modulators, $\psi_m(A; x, y)$ [18]. However the energy fluence must be related to the absorbed dose to be calculated in the TPS. To do this the direct energy fluence in air is separated into a reference energy fluence level, ψ_0 and a relative distribution function, $f(x, y)$. This distribution function represents the off axis energy fluence ratio of the direct beam energy fluence.

$$\psi_{dir}(x, y) = \psi_0 \cdot f(x, y) \quad (3)$$

The dose engines in the TPS yields internally dose per energy fluence. A dose engine is defined as d , i.e.

$$d(r) = \frac{D(r)}{\psi_0} \quad (4)$$

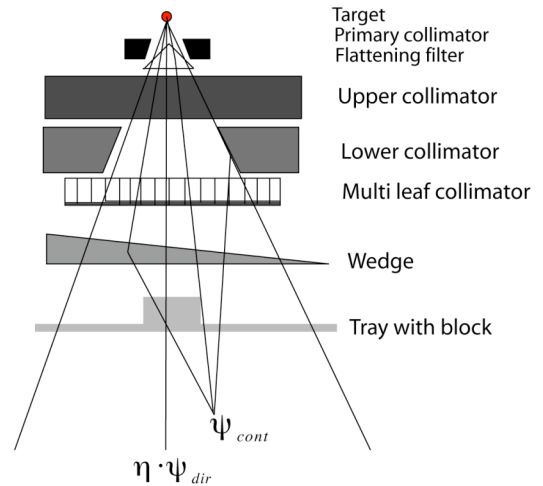


Figure 2.3:1
Graphical representation of a generic LINAC-head and its components

In this dose engine, $D(r)$ is the absolute absorbed dose at position \mathbf{r} . Hence the TPS calculates the absorbed dose considering all parameters such as irregular fields, different collimators, blocks, etc. [18].

Pencil Beam absorbed dose calculation

The pencil beam (PB) and the Collapsed Cone (CC) absorbed dose calculation algorithms are based on energy deposition kernels. These kernels describes the spread of dose from a primary interaction site [19]. Monte Carlo simulations are used to obtain these energy deposition kernels described by Mackie *et.al*, 1988. Theses mono energetic kernels are then convolved with an exponentially decreasing relative energy fluence. This is done to obtain a mono energetic pencil beam. Several of these mono energetic pencil beams are then compiled to a poly energetic pencil beam for each beam energy used [20]. These are compiled within the constraints of a beam spectrum model using a dual exponential for each depth according to the following relation:

$$p(z, r) = \frac{A_z e^{-a_z r} + B_z e^{-b_z r}}{r^2} \quad (5)$$

A_z, B_z, a_z and b_z are specific depth constants that are evaluated for each beam quality [21]. However there are limitations in this model in the build-up area. This discrepancy is assumed to be due to contaminating electrons and this is modeled using an decreasing exponential model [21].

To obtain the final absorbed dose distribution the energy fluence of the beam from the linear accelerator is convolved with the pencil beam. In equation 4 the absolute absorbed dose is related to the energy fluence and the dose engine, which is the pencil beam. Hence the absorbed dose distribution is calculated for any arbitrary field shape and modulation.

In the pencil beam concept are however some limitations. The main limitation is that the pencil beam algorithm calculates absorbed dose to water instead of absorbed dose to the actual medium irradiated. This is a consequence of the energy deposition kernels used which are calculated in water [7]. Corrections for inhomogeneities and elemental composition of materials along the beam path are being handled differently for different dose components in Oncentra master plan. These dose components are *primary dose*, *charged particle contamination dose*, *photon contamination dose* and *phantom scatter dose*. For the first three dose components the equivalent path length is used. This means that the depth dependant parameters are being evaluated at a calculation point in water corresponding to the radiological depth. The radiological depth is defined as the geometrical depth in water that the same attenuation would be found without any inhomogeneity i.e.

$$z_{rad} = z_{geom} \frac{\bar{\mu}}{\mu_{H_2O}} \quad (6)$$

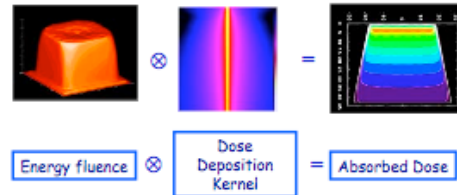


Figure 2.3:3

Illustration of a convolution of an energy fluence with a Monte Carlo generated dose deposition kernel (from T Knöös, with permission)

This method gives very precise results as long as lateral charged particle equilibrium is maintained. The expected error from these three dose components depends on the deviation from equilibrium conditions [18]. To calculate the phantom scatter dose a one dimensional convolution correction factor is multiplied to the resulting scatter dose to account for heterogeneities along the beam path [18].

Collapsed Cone absorbed dose calculation

The collapsed cone dose calculation algorithm is, unlike the pencil beam, volume oriented. In the collapsed cone a three-dimensional dose matrix is defined from the density geometry [18]. A ray-trace is performed from each of these voxel midpoints. This is done to determine how much radiant energy from the incident beam is deposited in each voxel. Effects of beam hardening and off-axis softening are included in the ray-trace and just like the pencil beam the absorbed dose is divided into primary dose and dose due to scatter [22]. By using this approach with a dose matrix in a density geometry the absorbed dose is calculated to the actual medium instead of water.

At each interaction site, the energy deposition and secondary particle transport is described by point kernels [22]. These point kernels as well as the mono energetic pencil beams are Monte Carlo-generated using a method described by Mackie *et.al* [19]. The data of these point kernels are parameterized by an exponential over r^2 , using the following relation:

$$h(r) = \frac{Ae^{-ar}}{r^2} \quad (7)$$

Where a describes the range of the energy transport from the interaction site. The ratio A/a equals the fraction of energy transported in the given direction per unit solid angle [18]. The parameterization is not uniformly distributed over the sphere of the point kernel. The parameterization is more pronounced in the forward direction, which is the direction that most secondary particles flow [19].

In the TPS used in this study, two sets of point kernels are used one for the primary dose and another one to yield the phantom scatter dose [18].

The dose integration over the dose matrix is from where the dose calculation has derived its name. In this integration it is assumed that all energy emitted in a solid angle cone is transported along the cone axis [22], hence the name, collapsed cone.

2.4 Implementation of X-Ray Computed Tomography in the TPS

CT-scanners are today widely used at radiotherapy departments all over the world. The use of a CT-scanner for radiotherapy has several advantages. The main advantages of a CT-scanner are to obtain physical information, like patient anatomy, size, shape and inhomogeneities; the other is to obtain the electron density from the different anatomical structures of the patient for the radiotherapy treatment planning [23].

The electron density is obtained from the CT-scanner via the so-called Hounsfield units (HU). These are defined as:

$$HU = 1000 \left(\frac{\mu - \mu_{water}}{\mu_{water}} \right) \quad (8)$$

Where μ is the linear attenuation coefficient for the respective material. The linear attenuation coefficient depends on parameters such as electron density, atomic number and the beam quality of the CT-scanner [23]. The linear attenuation coefficient can be expressed in form of the number of electrons per mass unit and the cross-sectional area per electron [24] *i.e.*

$$\mu = N_e \sigma_e \rho \quad (9)$$

Where N_e is the number of electrons per mass unit and σ_e is the cross section per electron. By substituting (9) into (8) yields the definition of Hounsfield number in expression of electron density *i.e.*

$$HU = 1000 \left(\frac{N_e \sigma_e \rho - N_{e,water} \sigma_{e,water} \rho_{water}}{N_{e,water} \sigma_{e,water} \rho_{water}} \right) \quad (10)$$

In the implementation of the Hounsfield scale in the TPS used in this study the Hounsfield scale stretches between $HU = -1000$ and $HU = 3000$. A HU of -992 represents air outside the patient and a HU of larger than 2832 represents iron [18]. However in the implementation of HU in this TPS the integers of the HU -scale are scaled according to the following relation to yield a byte array of 8-bit values for the density matrix [18]:

$$H_{DCM} = \frac{HU + 1000}{16} - 128 \quad (11)$$

The electron density is given in the TPS for a number of different materials of dosimetric interest [18]. Examples of these are muscle, cartilage, air, aluminum, et cetera.

The attenuation coefficient has to be known to calculate accurate Hounsfield numbers. The attenuation coefficient depends on several different factors as mentioned earlier. Uncertainty in determination of the attenuation coefficient can introduce an error that leads to an error in absorbed dose to the patient [23]. For a 6 MV radiotherapy beam an error in electron density of 8 % would lead to an error of 1 % in patient dosimetry [23]. However the study performed by Thomas has also proven that the significance of exact electron density

becomes less important with increased beam energy and higher atomic number (Z) and that this, somewhat, compensates for uncertainties in determination of Hounsfield number.

For a clinical beam of 6 MV the incoherent scattering process dominates [25]. However when irradiating materials of higher atomic number (Z) the contribution from pair production becomes significant. For muscle the ratio, incoherent scatter to pair production is 92/8 whilst it for compact bone is 89/11, this is given for an incident photon energy of 5 MeV [25]. This ratio also increases with increasing photon energy.

The implementation of electron density versus Hounsfield units in the TPS used in this study is calculated based on a method described by Knöös *et.al* [18].

2.5 Monte Carlo Simulations

The Monte Carlo method is a very powerful method to calculate absorbed dose distributions. By applying electron and photon interaction physics one can obtain an energy deposition from all incident particles on a three dimensional volume.

Every incident particle such as the electron, photon or any other particle that this incident particle sets in motion is referred to as a *history*. Each history is determined from a random selection from the probability distributions that control each possible interaction. Examples of probability distributions can be the distance to next interaction, cross section for photo electric effect, the Klein-Nishina cross section for Compton scattering etc. A dose distribution can be calculated by integrating the energy deposited in the region of interest by a summing of the histories and the particles associated with these histories. A very large number of histories are required to minimize the uncertainty and to allow reproducibility in the result [10].

The Monte Carlo method is very time consuming since all particles and their sub particles have to be simulated.

Several different Monte Carlo user programs and codes are available. In this study the EGSnrc user code DOSXYZnrc has been used to obtain the Monte Carlo simulated depth dose curves.

3. Materials and methods

The results obtained in this study are depth dose curves with and without dental material cavities. The measurements in the constructed phantom have been validated against a reference geometry phantom to assure an accurate output factor normalization of the results.

3.1 The phantom



Figure 3.1: 1

The 80x70x260 mm PMMA phantom with 5mm thick walls, a 1mm thick entrance window and two 45 mm thick PMMA slabs glued on the side for full scatter. There are 36 holes with a diameter of 5mm for TLD measurements.

For measurement of depth dose curves a purpose built phantom was created.

The main use of this phantom was to allow precise and accurate possibilities to measure depth doses. The phantom was created small and easy to use, but still with good precision to give accurate results when used. The material chosen for the phantom was *polymethyl methacrylate (PMMA)*. Since the ability to measure depth doses very precise is of utmost importance, the entrance window in the phantom was made very thin, 1 mm. Dental materials was placed in holes at predefined depths and in the holes behind or front, a rod was placed with a TLD placed in a milled track inside this rod. This rod was also made of PMMA (figure 3.1:2). To allow water to pass up through the TLD-rod two holes where drilled in the bottom of the TLD-rod.

For a closer spacing of the TLDs the phantom was constructed with 3 parallel lines of holes. These lines where shifted 3 mm in

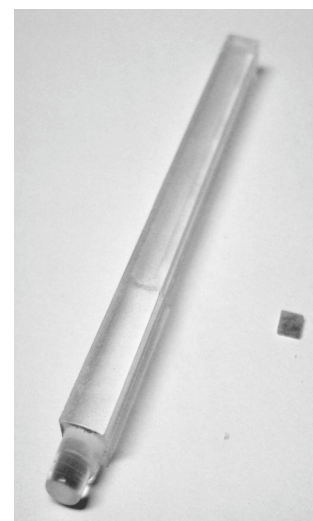


Figure 3.1:2
The TLD-rod

the longitudinal direction. The closest spacing between the measurements was 3 mm. A slab of PMMA was glued on both sides of the phantom to assure that full scatter was achieved when shifting measurement row.

The whole of the phantom and the TLD-rod was made waterproof. For the measurements, the phantom was filled with water to achieve electron equilibrium and to simulate human tissue. Water is almost always used as standard material for radiotherapy dosimetry.

An ionization chamber was used to validate the TLD result and a dedicated cradle was built to hold this ionization chamber (figure 3.1:3). To fixate the ionization chamber, two holes in the cradle was used. In the lower hole a plastic screw was placed to fixate the ionization chamber. The construction allowed for vertical movement of the ionization chamber in the phantom. This cradle was also built of PMMA (figure 3.1:3). The cradle was made so it could slide on the edges of the phantom. For accurate positioning of the ionization chamber a thin metallic pin was placed on the cradle at a position correspondent to the geometric center of the ionization chamber (figure 3.1:3, 3.2:1). A plastic ruler was placed on the PMMA slab on the right side of the phantom (figure 2.1:1). The ruler was held in position by two plastic screws.

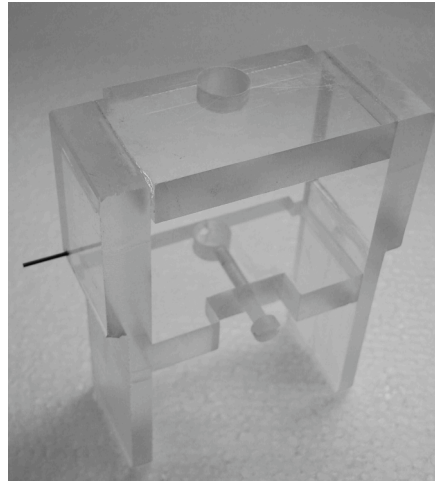


Figure 3.1:3 The cradle to house the ionization chamber

3.2 Beam geometry and measurement set up

Beam geometry

A beam of size $10 \times 10 \text{ cm}^2$ and with a SSD of 90 cm was used. The collimator of the accelerator was set at an angle of 0° and the gantry at 270° .

This beam geometry is also a part of the reference geometry used when measuring absorbed dose to water [26].

A photon beam energy of 6 MV was used in this study. This is an energy of clinical relevance in head and neck radiotherapy. For a beam energy of 6 MV the dose maximum lies at about 1.5 cm depth.

The dental materials were placed at 37 mm depth in the phantom, with 37 mm corresponding to the center of the dental materials. The height of the dental materials was set to the geometric center of the water filled part of the phantom.

TLD

TLDs were used to measure the depth dose curves. Each hole in the phantom was assigned a number and a TLD a corresponding number, this was done to allow a simple and accurate handling of TLD and position.

Monte Carlo Simulations

The Monte Carlo simulations were obtained using the EGSnrc user code DOSXYZnrc [27]. 3.000.000.000 histories were analyzed and dose was scored along the central axis in a 1 cm² circle perpendicular to the incident beam at distances of 2.5 mm. The Monte Carlo geometry was made equal to the real phantom. A simplified linear accelerator defined by Wieslander and Knöös [28] was used in the Monte Carlo simulations. The simplified accelerator uses a depth dose equivalent energy spectrum as input to the Monte Carlo simulation, which give a good agreement with measured data in water beyond the depth of maximum dose. This virtual accelerator has been validated for the accelerator used in this study [29].

Ionization chamber

The ionization chamber used in this study was the *Scanditronix Compact Camber CC01* (figure 3.2:1).

This chamber has a very small active volume, 0.01 cm³. This small active volume means that the over all size of the chamber is very small. It measures 48 mm in length with 10 mm diameter of the body. The tip, which holds the active volume is 3 mm in diameter. The ionization chamber is waterproof and gets ventilated by a plastic sleeve that contains the measuring cable. This compact design and the fact that it is waterproof made it suitable for these experiments.

The measurement data from the ionization chamber was output factor normalized.

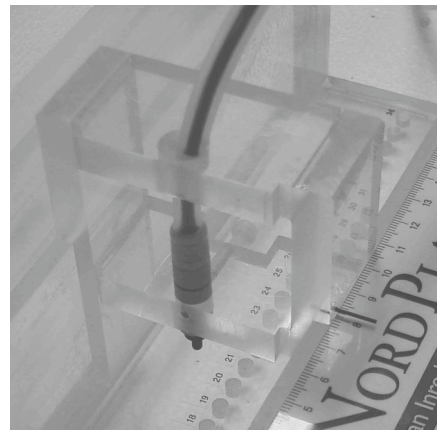


Figure 3.2:1 The cradle in the phantom with ionization chamber installed

The computer-generated phantom

A computer-generated phantom was created in the TPS. This phantom was made equal to the real phantom. Voxel sizes for absorbed dose calculations were 1 mm³.

The phantom was built up of four different ROIs. One ROI filled with water and three ROIs built of PMMA with density 1.19 gcm³ [30]. To simulate dental materials ROI's was added to the phantom at 37 mm depth in the center of the phantom. These ROIs were made 10x10x10 mm³. Only ceramic and porcelain ROIs was used. The TPS only handles custom densities below 2.83 gcm⁻³.

To validate that there was no difference between assigning a custom density and assigning the composition of the actual material a comparison was made. This comparison consisted of Al, Ca and C. No difference was found in the TPS between assigning the density or the atomic composition of these materials.

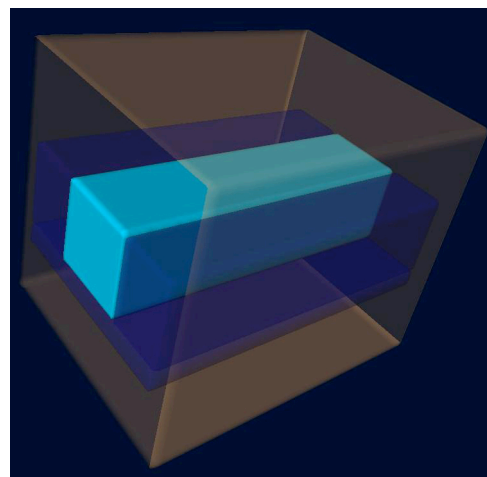


Figure 3.2:2 The computer generated phantom with water in the center

3.4 Radiotherapy equipment

Linear accelerator

The linear accelerator used in this study was a *Varian High Energy 2100 C/D Series Clinac* (Varian Medical Systems, Palo Alto, USA).

Treatment planning system

The treatment planning system that was used in this study was the commercially available *Oncentra Master Plan* (Oncentra Master Plan, version 1.5, Nucletron B.V, Veenendaal, The Netherlands).

CT-scanners

Two CT-scanners was used in this study. One CT-scanner that is used for radiotherapy treatment planning and another that is a pure diagnostic CT-scanner.

The CT-scanner that is used at the radiotherapy department is a *General Electrics HiSpeed NXi/Pro* (GE Medical Systems-Europe, Paris, France). This CT-scanner is a two-slice CT with possibilities for helical imaging. In this study the CT was operated in axial mode with an image acquisition of 2x1 mm slices. It was operated on 120 kVp and 200 mAs. The internal filtration of this CT-scanner is 6.32 mm aluminum equivalence at 70 kVp.

For comparison a more modern CT-scanner was used. This CT-scanner was a *Siemens Somatom Sensation 64* (Siemens, Germany). This CT-scanner is a multi-slice CT with 64 slices. The CT was operated in axial mode with an image acquisition of 2x1 mm slices. It was operated on 120 kVp and 200 mAs. The internal filtration of this CT-scanner is equivalent to a half value layer correspondent to 6.8 mm Al \pm 0.2 mm Al. This is given for a potential of 80 kV.

3.5 Dental materials

A number of different dental materials of clinical relevance were chosen for this study. Other dental materials such as different Cobalt Chrome alloys and Amalgam are also of clinical relevance [5]. However due to economic reasons cobalt-chrome was not evaluated. Amalgam is an alloy that contains mercury and is nowadays not used in Sweden [5]. Because of this the material could not be obtained. All dental materials except the titanium were obtained from a local dental laboratory, DPNova [DPNova, Malmö, Sweden]. Manufacturing porcelain and composites with precise cubic dimensions is difficult due to the burning process. Perfectly cubic dimensions can be obtained by using a computer aided milling machine. DPNova does not utilize this kind of equipment in their manufacturing process. The dimensions of the dental materials are given in table 3.5:1. Note that composite and porcelain are not perfectly cubic. The effect on the final dose distributions due to the lack of perfect cubic dimensions can be neglected. The coordinate system used is the same as the coordinate system for the TPS which means that the x-z-direction is perpendicular to the incident beam [18].

Table 3.5:1 *Dimensions of dental materials*

Material	Dimensions (mm)		
	x	y	z
Composite	10.0	10.7	10.1
Porcelain	10.9	8.6	11.5
Titanium	10.0	10.0	10.0
Gold	8.0	4.0	8.0

Gold

The gold alloy used in this study is the *Heranordic 75* [Heraeus Kulzer GmbH, Hanau, Germany]. This alloy consists of 75 % Au, 1.3 % Ag, 17.9 % Pd, 1.0 % Sn, 0.2 % Zn, 4.5 % In and less than 0.1 % Ir and Ru. These percentages are given in fraction by weight. The density of the gold alloy is 16.1 gcm^{-3} .

Porcelain

The porcelain used in this study is the *HeraCeram* [Heraeus Kulzer GmbH, Hanau, Germany]. This porcelain has a density of 2.5 gcm^{-3} . The composition of this porcelain is not specified. Monte Carlo simulations for the porcelain has not been obtained.

Composite

The composite used in this study is the *3M ESPE Sinfony Paste* [3M Svenska AB, Sollentuna, Sweden]. This composite like the HeraCeram has no detailed specification of the elemental composition. The density of the composite is 1.5 gcm^{-3} . For the Monte-Carlo simulations this composite has been approximated with PVC. The elemental composition of the PVC is 4.8 % H, 38.4 % C and 56.7 % Cl. This PVC has a density of 1.3 gcm^{-3} [31].

Titanium

The titanium used in this study is a pure titanium slab with density 4.54 gcm^{-3} .

4. Results and discussion

The results of most interest are presented in this chapter. However the complete depth dose curves are presented in Appendix 1.

4.1 Evaluation of measurement method and uncertainties

The comparison with TLD and the compact ion chamber shows a much better agreement with the Monte Carlo calculated depth dose curve in favor for the compact ion chamber (figure 4.1:1).

Due to technical problems with the TLD reader two deviating points from the TLD measurements have been removed. These two points showed a difference in absolute signal that cannot be attributed to any set-up error. Due to the same technical problems the measurements could not be repeated. This further justifies the removal of the erroneous data points.

The uncertainties in these results have been estimated using standard uncertainties of *type A* described according to the International Standard Organization. The method used has been obtained from IAEA technical report series [26]. For the TLD result the uncertainty was calculated only for the uncertainty in the central depth dose. For the compact ion chamber, uncertainty in position was also taken into account. This uncertainty was calculated as the difference in absorbed dose around the point at 10 cm depth as a *type A* standard uncertainty. The uncertainty in positioning of the compact ion chamber was estimated to 0.5 mm. This was combined with the uncertainty in the central depth dose measured with the compact ion chamber [26]. The corresponding standard uncertainty for TLD at 10 cm depth was 1.6 % and for the compact ion chamber at 10 cm depth the standard uncertainty was 0.46 %, which further supports the use of the compact ion chamber.

When comparing the Monte Carlo simulations with TLD and the compact ion chamber it is obvious that the superior measuring method is with the compact ion chamber. All results from here on are obtained with the compact ion chamber.

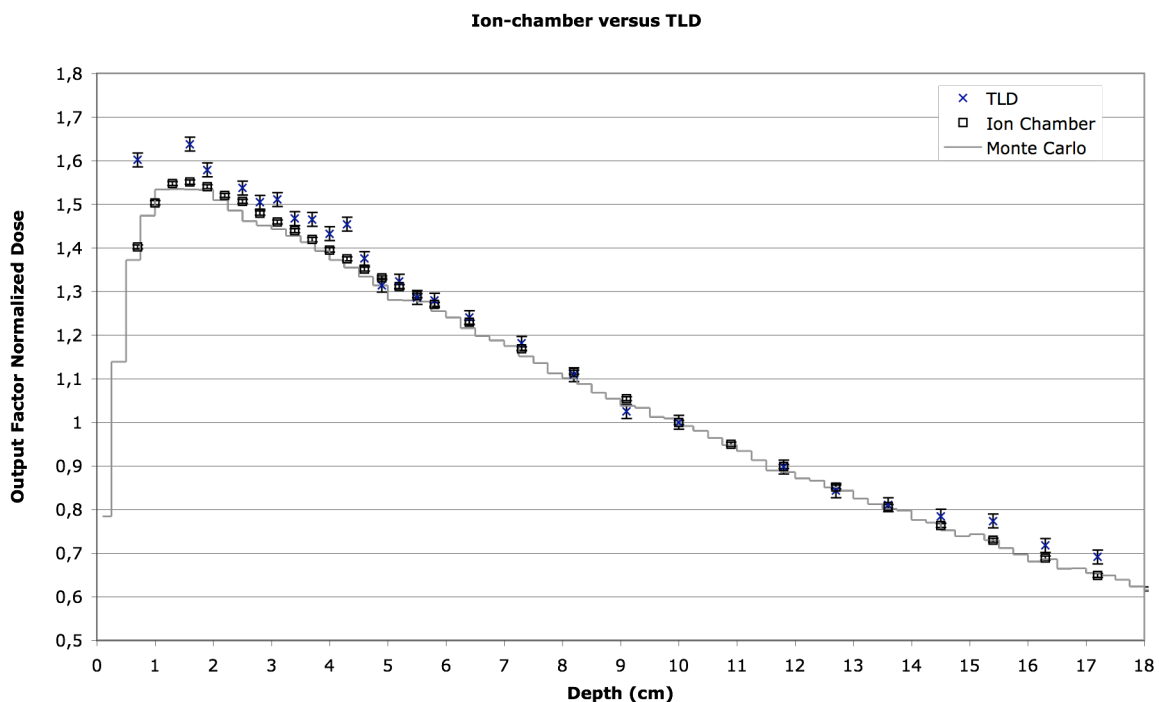


Figure 4.1:1 Comparison between TLD and Ion chamber with a Monte Carlo simulated depth dose curve

4.2 Comparison between the computer-generated phantom, ion-chamber measurements and CT-scanner in water

The TPS clearly underestimates the absorbed dose when calculating the absorbed dose from the data of the CT-scanner (figure 4.2:1).

There was a difference of 2.7 % in absorbed dose between the CT-scanner and the computer-generated phantom at 10 cm depth (figure 4.2:1). The TPS internally assigns a mixture of adipose/tissue to the CT-scanned phantom. This mixture has a density of 1.02 gm^{-3} , which is 2 % lower than density of water [18]. The density of the water slab in the computer-generated phantom was set to 1.00 gm^{-3} . This custom assigned density yielded a result comparable to the measurements with the ionization chamber. The difference between measurements and CT-scanner obtained density information is not unexpected since the reference manual for the TPS clearly states that there is this difference. However it is of importance to show the difference for users not aware of this limitation and assuming that the TPS calculates the absorbed dose to water when water is CT-scanned. The difference between the ionization chamber measurements and the computer-generated phantom in the build-up area can be attributed to the normalization method.

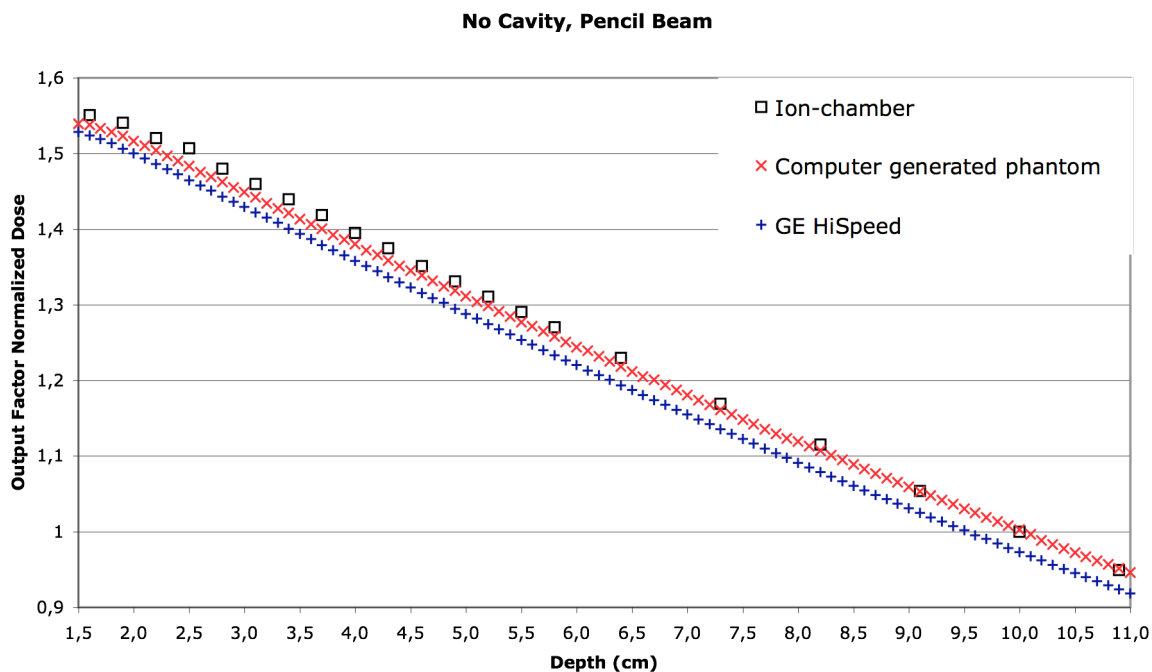


Figure 4.2:1 Comparison between the computer-generated phantom, ion chamber and the GE CT-scanner without dental cavity. Evaluated using pencil beam

4.3 Evaluation of depth dose curve for gold alloy

The limitations in the TPS are obvious when evaluating the depth dose curve for a high-density material. The absorbed dose is both overestimated and underestimated.

The high density and atomic composition of the gold alloy leads to a 23 % difference in absorbed dose just before the gold alloy cavity compared to the dose maximum at 1.5 cm depth (figure 4.3:1). The difference in absorbed dose after the dental material cavity is also overestimated. The overestimation at 5 cm depth is 5 % (figure 4.3:1). The overestimation prior to the cavity like the titanium (figure 4.4:1) is due to contaminating electron originating from the high-density material [6]. The fact that the gold alloy used in this study has a density of 16.1 gcm^{-3} compared to titanium, which has a density of 4.54 gcm^{-3} explains why the build up of dose before the cavity is this much larger. The difference in absorbed dose after the cavity is an effect of the density assigned to the CT-data from the TPS. The maximum density handled in the TPS used in this study is 7.87 gcm^{-3} , which is the density of iron. The underestimation of density leads to this underestimation of absorbed dose after the dental material cavity.

At 10 cm depth and deeper all depth dose curves are coinciding. The clinical relevance of this is not significant since the distance from the dental material cavity is too large. The regions of interest for patient dosimetry are the regions just before and after the cavity. In these regions the TPS calculated results significantly differ from the measured data.

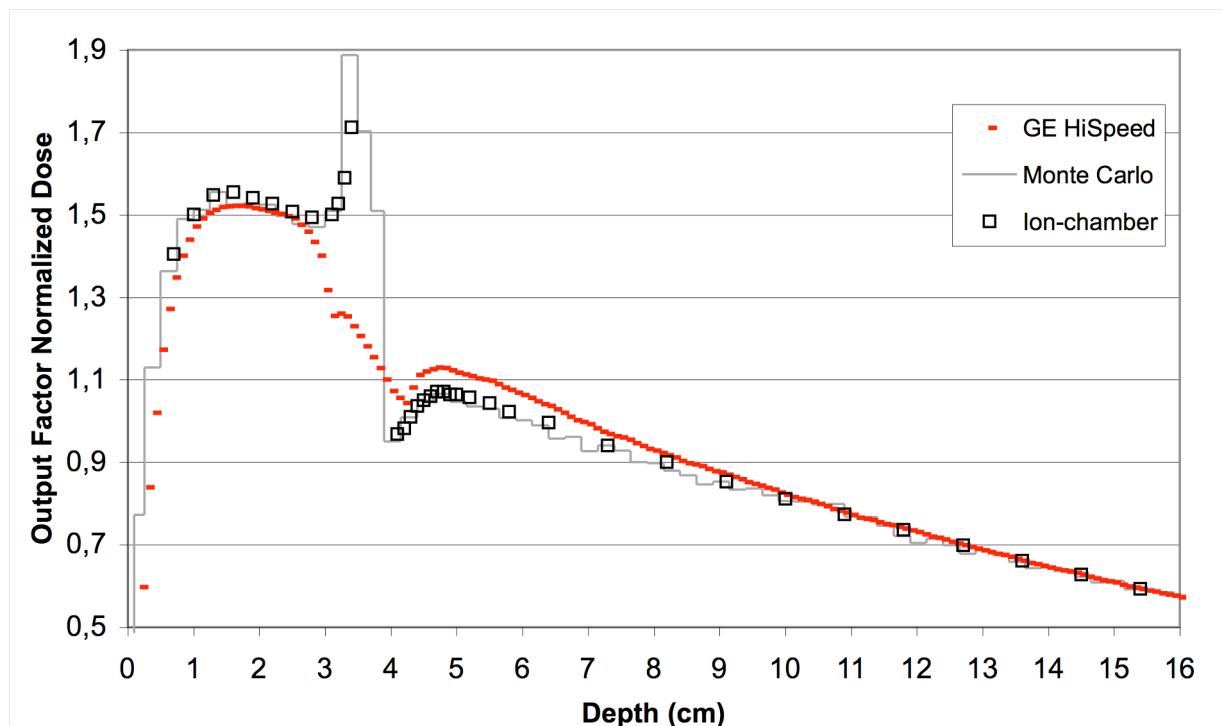


Figure 4.3:1 Depth dose curve for gold alloy evaluated using the collapsed cone absorbed dose calculation algorithm

4.4 Difference between the pencil beam and collapsed cone calculation algorithm.

After a high-density cavity the TPS underestimates the absorbed dose for both the pencil beam and the collapsed cone calculation algorithm. There is also a clear difference between the pencil beam and the collapsed cone calculation algorithm in and beyond the high-density cavity.

A difference of 8.8 % between the pencil beam and the collapsed cone in the center of the cavity at 37 mm depth was found when evaluating the absorbed dose distributions (figure 4.4:1). The difference between the Monte Carlo simulation and the collapsed cone algorithm was 1.1 % at the same depth. This result supports the conclusion that the collapsed cone algorithm is preferable algorithm of the two [7]. The difference between the pencil beam algorithm and the collapsed cone algorithm is due to the intrinsic properties of the different calculation algorithms. The collapsed cone calculates absorbed dose to the actual medium where as the pencil beam only calculates absorbed dose to water but with a correction factor for the equivalent path length included [7]. The collapsed cone also models the build up after the dental material cavity, although not completely. The titanium slab is calculated denser than the actual density in the TPS, this means that there is an underestimation of the absorbed dose after the dental material cavity. None of these two absorbed dose calculation algorithms calculates the build up of dose in front of the cavity. The absorbed dose build up in front of the cavity is due to contaminating electrons back scattered from the high-density cavity [6]. The contribution of these contaminating electrons increases with increased density of the dental material cavity.

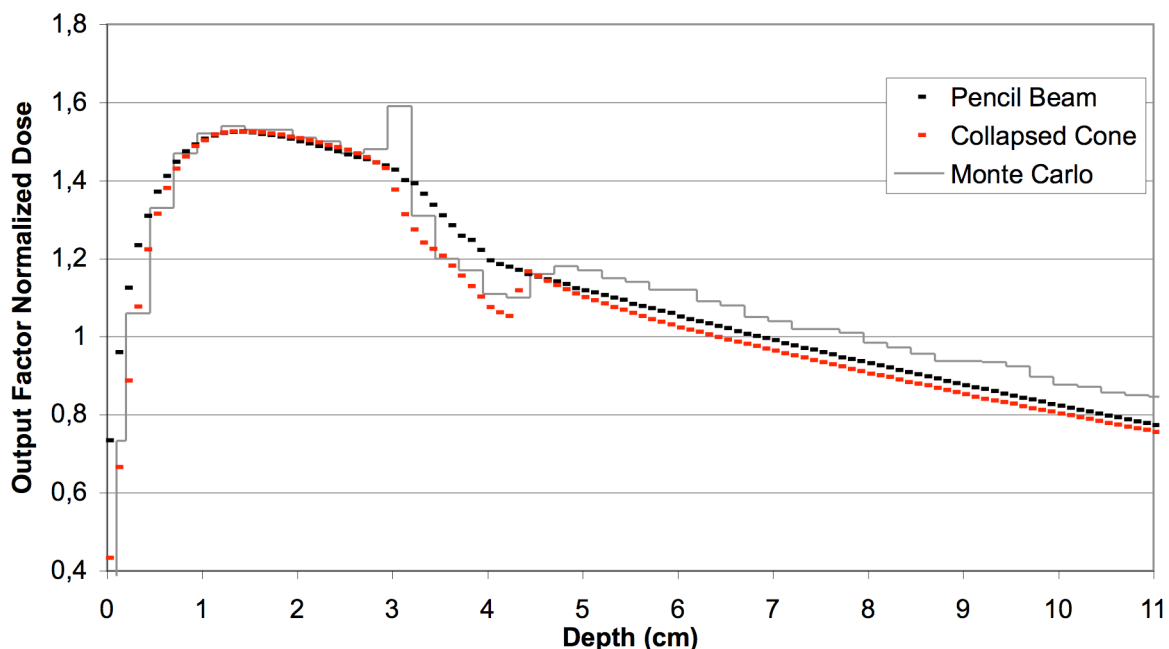


Figure 4.4:1 Comparison between the pencil beam and the collapsed cone calculation algorithms evaluated for titanium cavity in the ct-scanned phantom

4.5 Evaluation of Hounsfield number implementation in the TPS

The TPS assigns the electron density to Hounsfield numbers from a pre defined look-up table [18]. In this table material of dosimetric interest are presented. When comparing the Hounsfield scale obtained from this table with the Hounsfield numbers obtained from the CT scanned phantom with different dental materials a large discrepancy was found (figure 4.5:1). The most recent quality assurance protocol (2006-05-09) for the GE HiSpeed CT was studied and valid in the range up to 1000 HU (table 4.5:1). Beyond 1000 HU no QA-measurement is available.

The underestimation of Hounsfield number will lead to an overestimation of density. Thus the absorbed dose after the dental material cavity is underestimated (figure 4.4:1, figure 4.6:1). The result from the titanium slab has not been evaluated in figure 4.4:1. This due to the assigning of a Hounsfield number larger than 2832, which means that the material is interpret as iron [18] and the absorbed dose is underestimated beyond the high-density cavity. For the gold alloy an overestimation of absorbed dose can be expected due to the same reason.

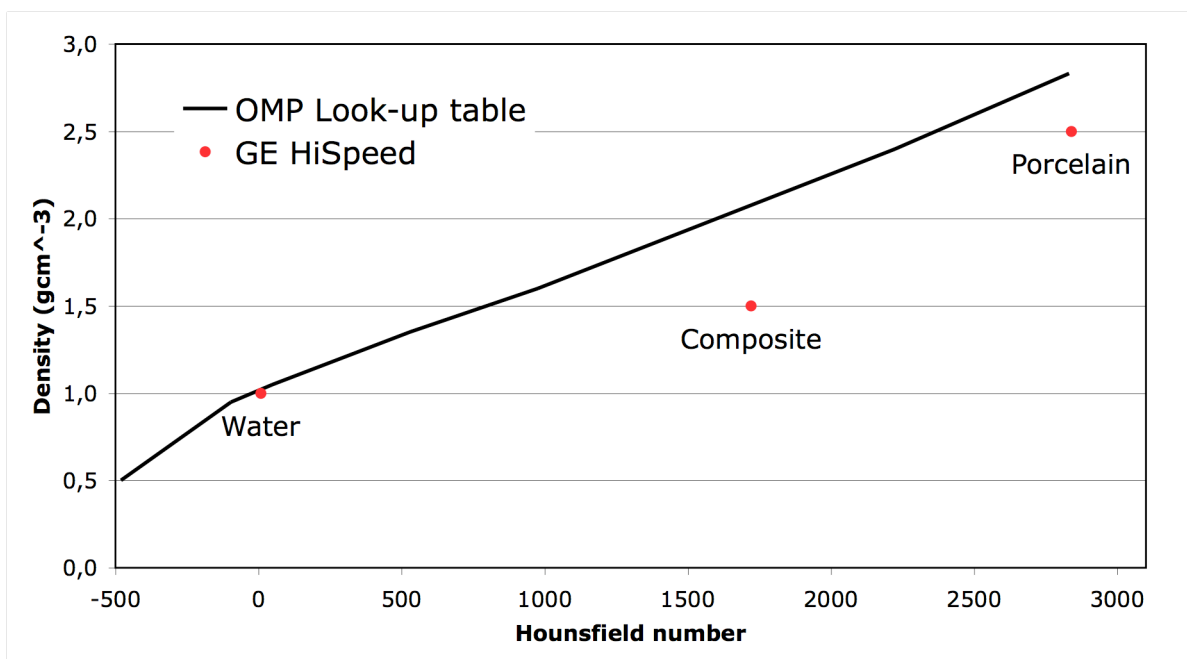


Figure 4.5:1 Comparison between Hounsfield units from predefined materials in the TPS with measured Hounsfield units with the GE HiSpeed CT scanner

Table 4.5:1 QA control 06-05-09

Material	Hounsfield number	
	Measured	Reference
Air	-996,11	-1000
Nylon	-83,6	-85
Plexiglass	127,63	126
Teflon	944,13	948

4.6 Comparison between CT-scanned phantom and computer-generated phantom for porcelain

The dental porcelain used in this study has a density of 2.5 gcm^{-3} . This density has also been assigned to a custom defined ROI in the computer-generated phantom simulating the dental material cavity. There was an underestimation of dose after the porcelain cavity compared to the computer-generated phantom when evaluating the CT-scanned phantom (figure 4.6:1). This underestimation is 4.7 % at 5 cm depth and is caused by an overestimation of density in the TPS from the HU-numbers in the CT-data. The TPS assigns the density of iron (7.87 gcm^{-3}) if the HU-number is larger than 2832 [18]. When assigning the density of porcelain to the dental cavity ROI in the computer-generated phantom a correct result is obtained. However build-up before and after the dental cavity is not handled correctly in the TPS as described earlier.

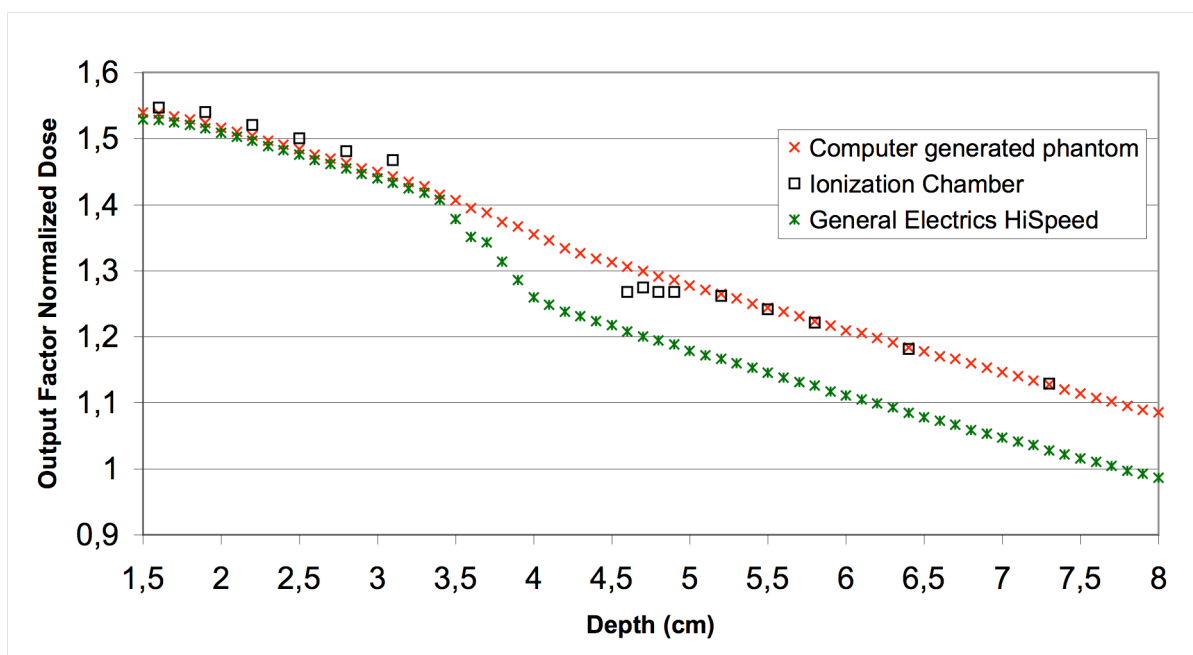


Figure 4.6:1 Comparison between the ct-scanned phantom and the computer-generated phantom evaluated for porcelain cavity using pencil beam

4.7 Comparison between two CT-scanners

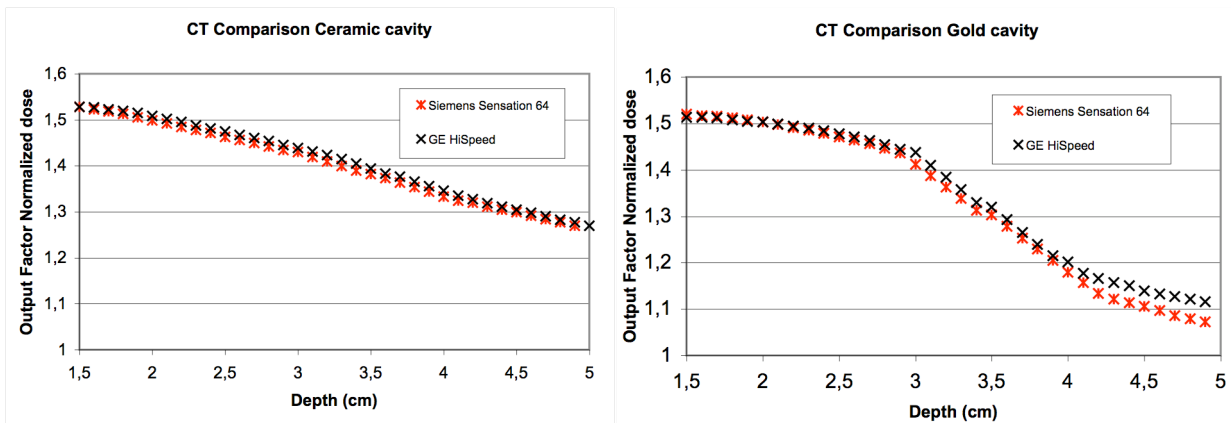


Figure 4.7:1 TPS calculated depth doses for two different CT-scanners and plotted for ceramic cavity (left) and gold cavity (right)

The effect of the different CT-scanners on the absorbed dose distributions was studied using the pencil beam calculation algorithm. The difference increased in calculated absorbed dose from the TPS between the two CT-scanners with increasing density of the cavity (figure 4.7:1). This difference was not dependant on the calculation algorithm used (Appendix 1, figure A.1.2 and figure A.2.8). At 4.5 cm depth the difference in pencil beam calculated absorbed dose between the two CT scanners was 3.0 %. This difference is dependant on several factors. One contributing factor is the reconstruction artifacts due to the high-density material (figure 4.7:2). These artifacts can be attributed to reconstruction filters used in the reconstruction of the CT-image and beam hardening effect. The two CT-scanners used in this study have different internal filtrations. The filtration of the Siemens Sensation is harder than the filtration for the GE HiSpeed. This means that the result derived from the Siemens Sensation yield better results than the GE HiSpeed (Appendix 1, figure A.1.8).

Since the TPS calculates the absorbed dose distributions from the density matrix defined by the CT-study this means that an error in the image such as an artifact yields an error in the dose calculation. These artifacts also yield an error in determining the correct thickness of the gold slab. The gold slab is 4 mm thick and centered around the depth of 37 mm. In the CT-study the gold slab is interpret as 10 mm thick.

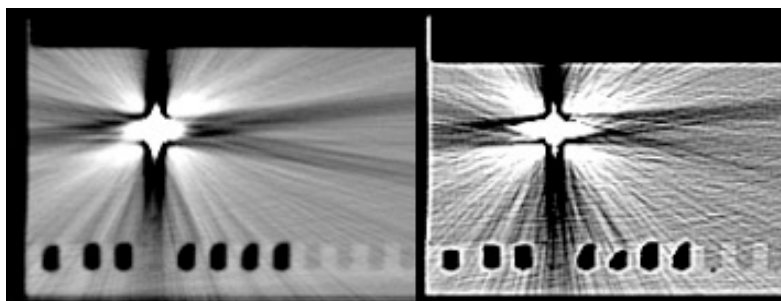


Figure 4.7:2 CT images of the gold alloy from the GE HiSpeed on the (left) and Siemens Sensation 64 on the (right)

5. General Discussion

The results obtained in this study show that there are large discrepancies between the TPS calculated and the measured absorbed dose distributions in front and beyond the dental materials. This study further supports previous studies performed by other authors in this area [6, 7]. In addition the errors introduced by the CT-scanner has been quantified.

One of the aims of this study was to quantify the contribution to the dose distribution from the back-scattered contaminating electrons when irradiating high-density materials [6]. A large build-up of dose due to contaminating electrons was found when irradiating the gold alloy and the titanium slab (figure 4.3:1, figure 4.4:1). One must take this into account when doing treatment planning for head and neck cancer with high-density materials present. The best way to prevent the excess dose in the vicinity of the high-density dental material is to increase the distance between the dental material and the surrounding oral tissue. The best way to obtain this difference to the oral tissue is to use bite-blocks. The use of bite-blocks is also a good way to fixate the patient during the treatment for an optimal treatment. [11].

The effect on the total uncertainty in obtaining a correct dose distribution from the CT based treatment planning cannot be neglected (figure 4.5:1). According to the quality assurance program for the GE HiSpeed CT used in this study the conversion of Hounsfield numbers for the TPS should be valid of up to density of approximately 1.6 gcm^{-3} (table 4.5:1). The results obtained from CT scanning of the dental materials in this study show a discrepancy of approximately 700 HU (figure 4.5:1). What this effect is dependant on must be further investigated. However the effect of this difference must not be neglected when doing treatment planning because this effect leads to an underestimation of absorbed dose beyond a dental material cavity. The effect of the CT scanner on this dose distribution is most relevant for materials with density lower than aluminum (2.83 gcm^{-3}). For higher density materials the limitation of the treatment planning system becomes a contributing factor (figure 4.4:1, figure 4.6:1). There is also a need to validate a CT scanner prior to commissioning for radiotherapy treatment planning since two different brands of CT scanners produce different results (figure 4.7:1). The impact of different reconstruction filters in the CT scanners has not been evaluated in this study. However the difference in the images obtained from the two CT scanners indicates that this is a potential source of uncertainty (figure 4.7:2). Thus there is also a need to validate the impact of different reconstruction filters before commissioning a new CT scanner. The methods described in this study could be used for obtaining these validations.

Although good built in functions for custom defining phantom the main limitation in the TPS lies in the assigning of density to ROIs. The highest density that one can assign to a custom defined ROI is 2.83 gcm^{-3} . This makes comparison between measurements impossible if density of the material of interest is denser than aluminum. In this study assigning of density up to 2.5 gcm^{-3} yields results very similar to results obtained from measurements. Another limitation in the TPS that is of relevance for clinical use is a limitation in the ROI catalog. In the TPS one can create predefined ROIs in a catalog. This is done to simplify the use of ROIs. However, if a ROI in the catalog is changed the TPS does not update the ROIs in the treatment plan with this change. This limitation can result in miscalculations and result in an administered absorbed dose to a patient that is not optimal. Users of this TPS must be aware of this limitation.

6. Conclusions

Large discrepancies of up to 23% in absorbed dose were found in the area just in front of the high-density dental material cavity. Both the collapsed cone algorithm and the pencil beam algorithm failed to calculate this build-up of dose in front of a high-density cavity. However by using bite-blocks to increase the distance between the dental material and oral tissue the dose contribution owing to these contaminating electrons will be significantly lower.

The difference in absorbed dose between the two calculation algorithms was up to 8.8 % in the dental material cavity, whereas the difference between the collapsed cone algorithm and reference Monte Carlo simulations was only 1.1 %. This leads to the conclusion that the collapsed cone is the preferable calculation algorithm, by other authors also stated [7].

The CT scanner used for obtaining treatment-planning data shows a significant impact on the final dose distribution. For the medium density dental material porcelain the underestimation of absorbed dose after the dental material cavity was 4.7 % and for the gold alloy an overestimation of dose at 5 cm depth was 5 %. Also a difference of 3 % in absorbed dose beyond the cavity was found between two different CT scanners when evaluating the gold alloy dental material.

An evaluation of the Hounsfield numbers in the center of the CT scanned dental material cavity showed a difference of up to 700 HU compared to the look-up table for Hounsfield units in the TPS (figure 4.5:1). This difference will lead to an over or underestimation of absorbed dose after a high-density material cavity. The origin of this difference has to be further studied. However the physician must take this effect into consideration when evaluating the patient's treatment plan.

7. Acknowledgements

This study could not have been carried out if it had not been for the help of the following persons: Thus I would like to thank my supervisors Sven Bäck, Lena Wittgren and Göran Bjelkengren for all help and support in carrying out this study. Further I would like to thank Sven Brink for help with building phantoms, Elinore Wieslander for great work in obtaining Monte Carlo simulations, Mikael Gunnarsson for help with CT-scanners and Erik Strandman for help with the choice of dental materials. A very special thanks dedicated to the personnel at DP-Nova dental laboratory and especially to Christer Edenfjord for help with manufacturing of dental materials.

Appendix 1: Depth dose curves of dental materials

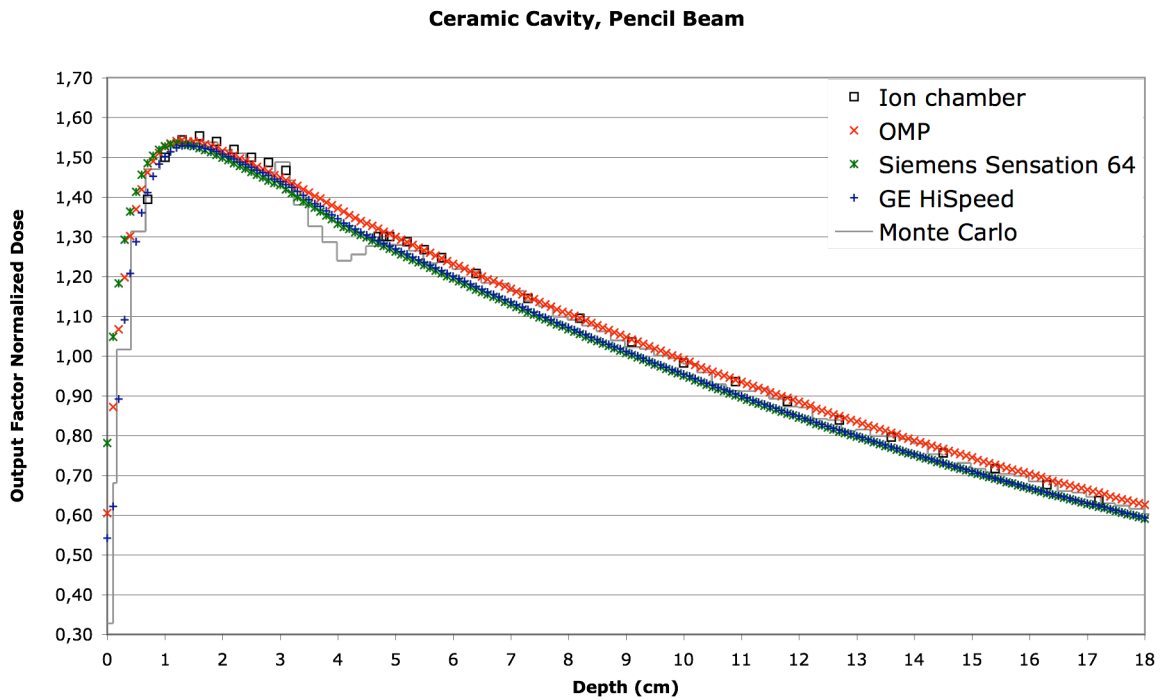


Figure A.1.1: Depth dose curve for ceramic cavity calculated using pencil beam

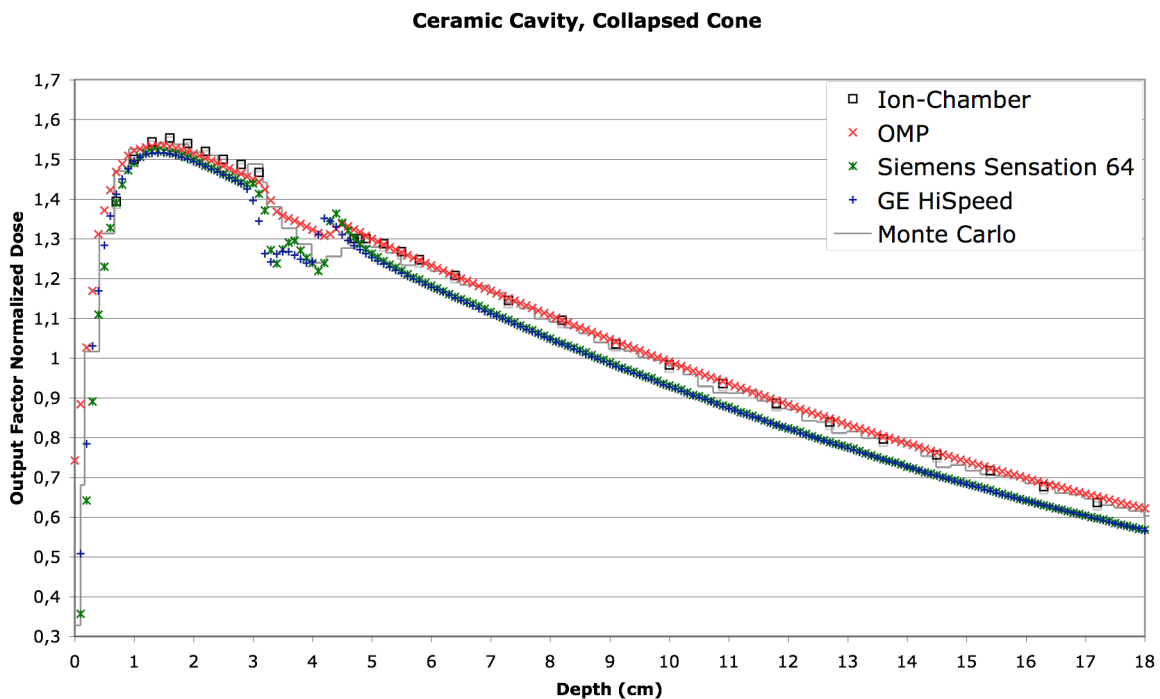


Figure A.1.2 Depth dose curve for ceramic cavity calculated using collapsed cone

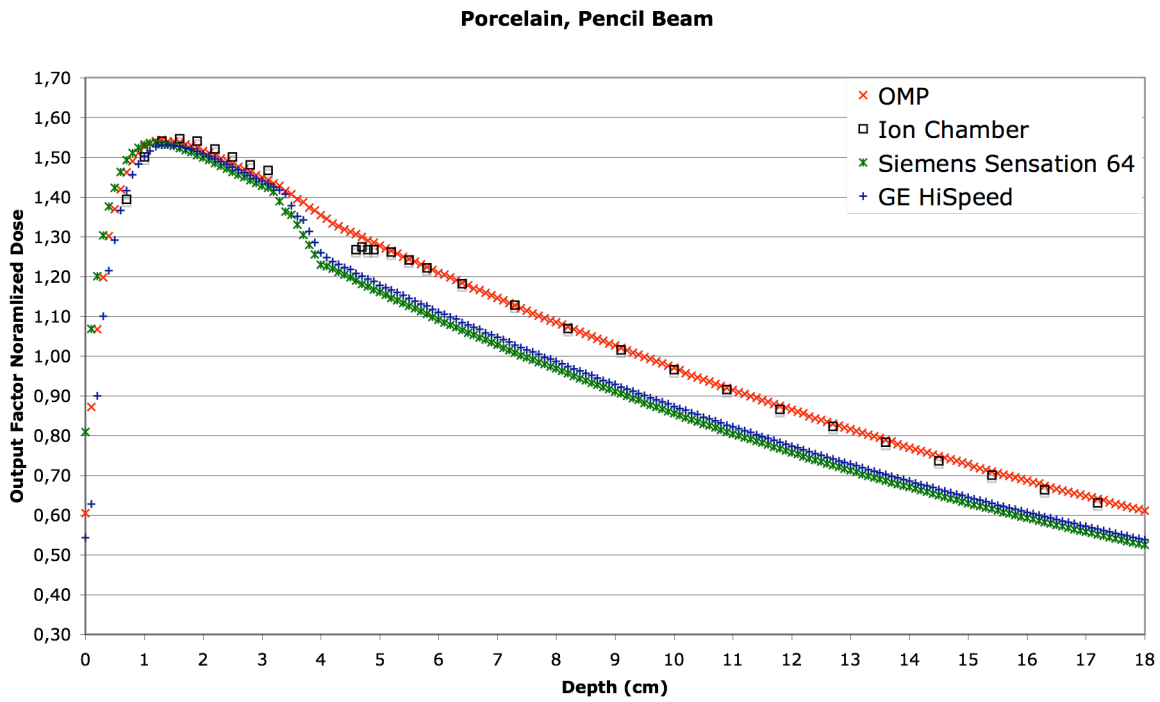


Figure A.1.3 Depth dose curve for Porcelain cavity calculated using pencil beam

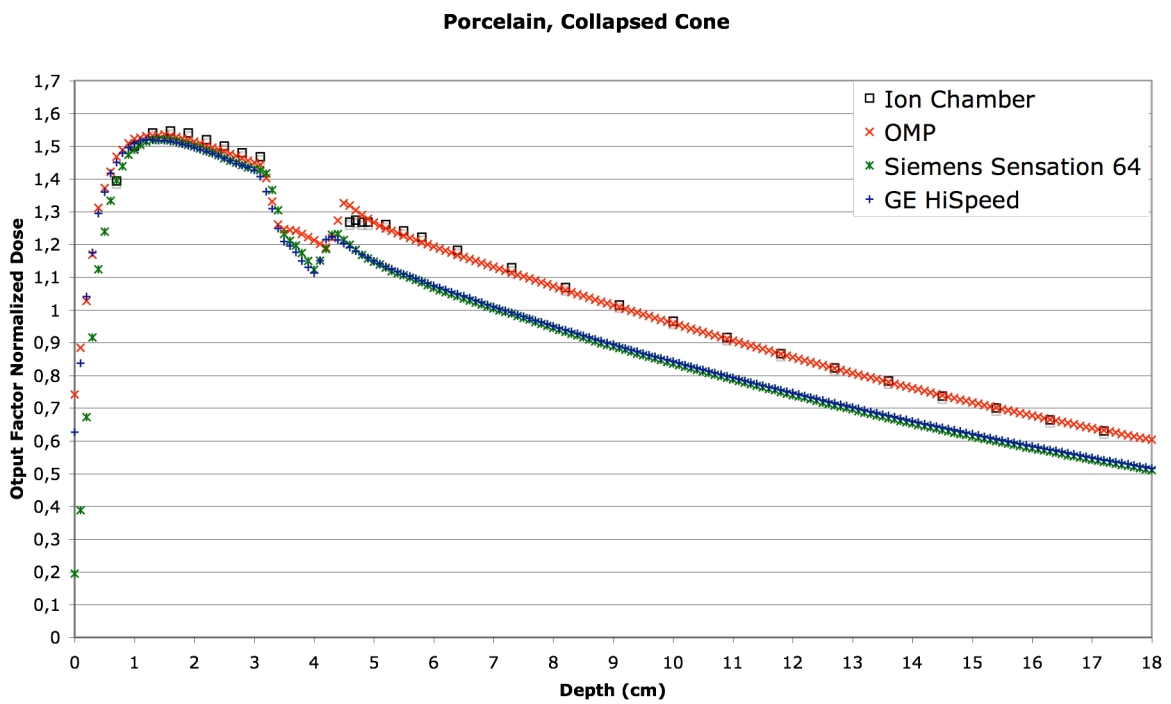


Figure A.1.4 Depth dose curve for porcelain cavity calculated using collapsed cone

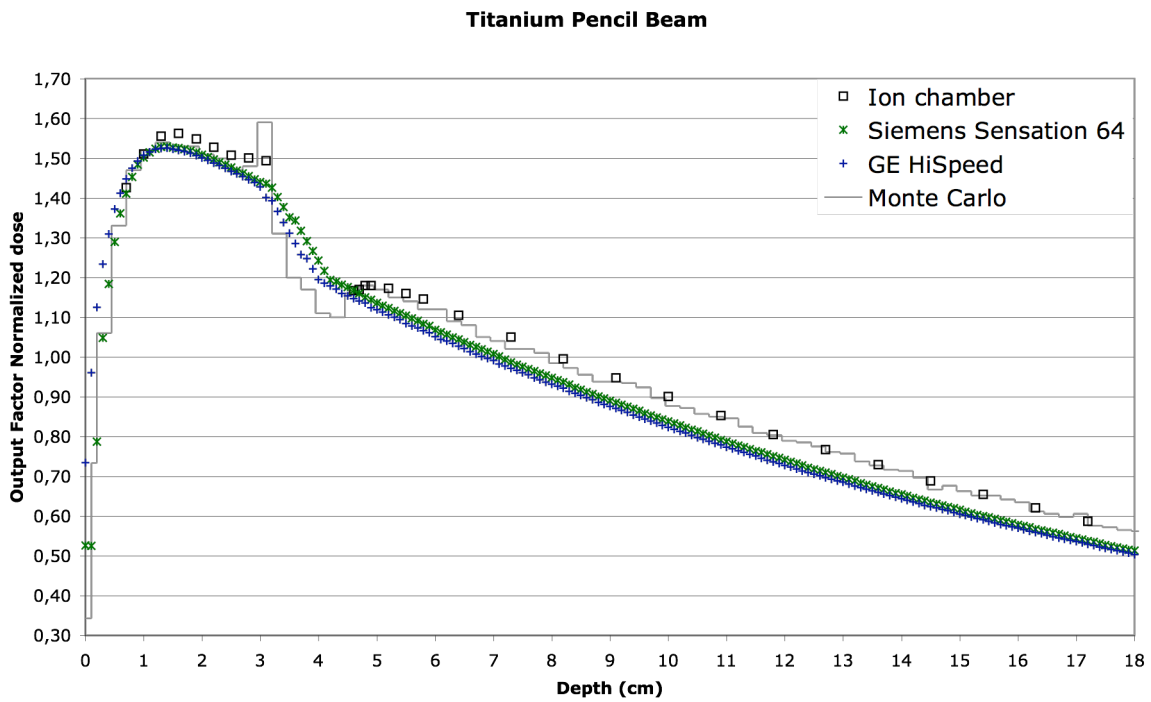


Figure A.1.5 Depth dose curve for titanium cavity calculated using pencil beam

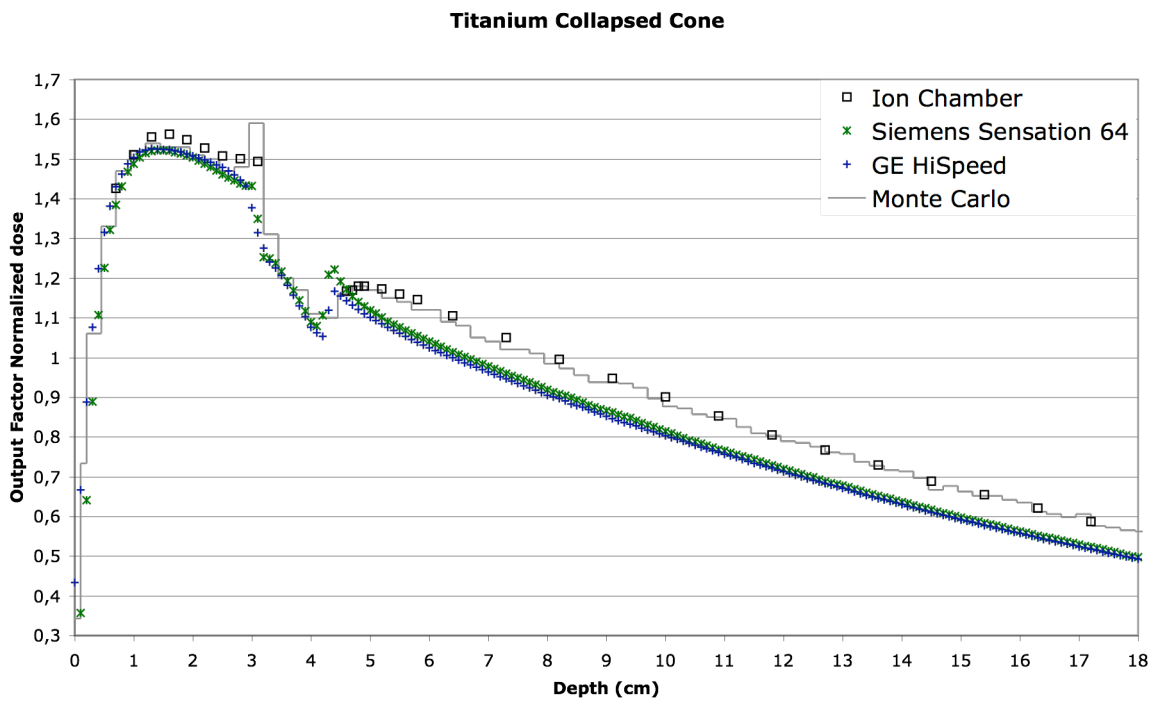


Figure A.1.6 Depth dose curve for titanium cavity calculated using collapsed cone

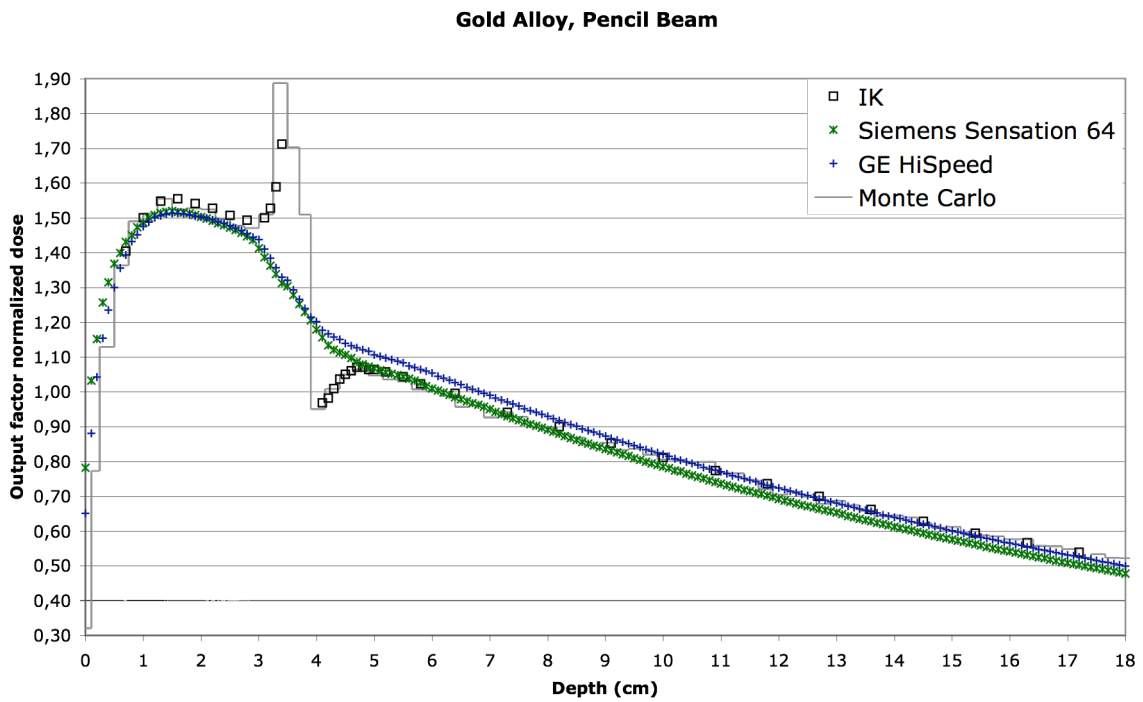


Figure A.1.7 Depth dose curve for gold alloy cavity calculated using pencil beam

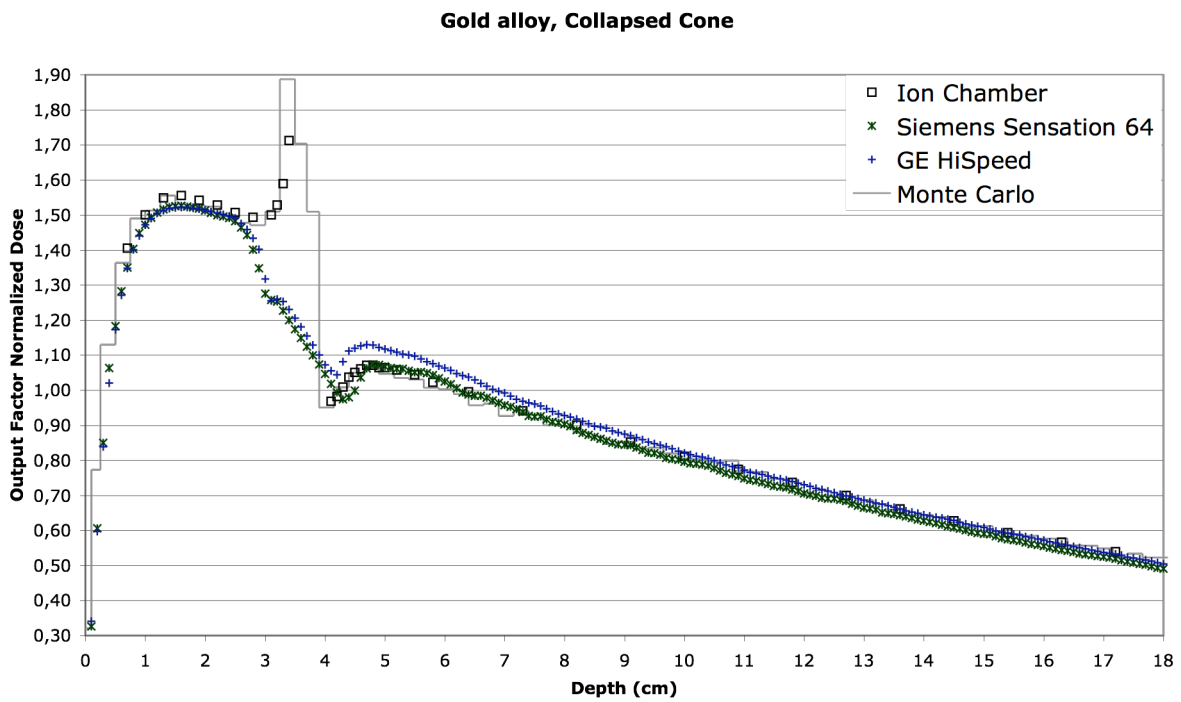


Figure A.1.8 Depth dose curve for gold alloy cavity calculated using collapsed cone

References

1. Socialstyrelsen, *Cancer incidence in sweden 2004*. 2004.
2. Vissink, A., J. Jansma, F.K. Spijkervet, F.R. Burlage, and R.P. Coppes, *Oral sequelae of head and neck radiotherapy*. Crit Rev Oral Biol Med, 2003. **14**(3): p. 199-212.
3. Hall, E.J., *Radiobiology for the radiologist*. 5. ed. 2000, Philadelphia: Lippincott Williams & Wilkins. xi, 588.
4. Bodil Fagerberg-Mohlin, C.-G.E., Karl-Erik Kahnberg, *Orala problem vid tumörbehandling inom huvud-halsregionen*. Tandläkartidningen, 2000. **92**(13).
5. Dérand, T. and M. Molin, *Dentala material : bra att veta i klinisk vardag*. 1. uppl. ed. 2004, Stockholm: Gothia. 194.
6. Spiriyovich, S., L. Papiez, M. Langer, G. Sandison, and V. Thai, *High density dental materials and radiotherapy planning: comparison of the dose predictions using superposition algorithm and fluence map Monte Carlo method with radiochromic film measurements*. Radiother Oncol, 2006. **81**(3): p. 309-14.
7. Wieslander, E. and T. Knoos, *Dose perturbation in the presence of metallic implants: treatment planning system versus Monte Carlo simulations*. Phys Med Biol, 2003. **48**(20): p. 3295-305.
8. SBU, *Strålbehandling i Sverige*. Vol. Rapport nr 162. 2003.
9. *Vårdprogram för cancer inom huvud-halsregionen*. 2005, Lund: Onkologiskt centrum.
10. Metcalfe, P., T. Kron, and P. Hoban, *The physics of radiotherapy X-rays from linear accelerators*. 1997, Madison, Wis.: Medical Physics Publ. xi, 493.
11. Karger, C.P., O. Jakel, J. Debus, S. Kuhn, and G.H. Hartmann, *Three-dimensional accuracy and interfractional reproducibility of patient fixation and positioning using a stereotactic head mask system*. Int J Radiat Oncol Biol Phys, 2001. **49**(5): p. 1493-504.
12. Willner, J., U. Hadinger, M. Neumann, F.J. Schwab, K. Bratengeier, and M. Flentje, *Three dimensional variability in patient positioning using bite block immobilization in 3D-conformal radiation treatment for ENT-tumors*. Radiother Oncol, 1997. **43**(3): p. 315-21.
13. International Commission on Radiation Units and Measurements, *Prescribing, recording, and reporting electron beam therapy*. Journal of the ICRU, 4(2004):1. 2004, Oxford: Oxford University Press. 100.
14. Andrews, N. and C. Griffiths, *Dental complications of head and neck radiotherapy: Part 1*. Aust Dent J, 2001. **46**(2): p. 88-94.
15. Ingrid Hofmann, H.Q., *Strålbehandling med inriktning mot tumörer i huvud-halsregionen*, in *Odontologiska fakulteten*. 2004, Malmö högskola: Malmö. p. 19.
16. Hancock, P.J., J.B. Epstein, and G.R. Sadler, *Oral and dental management related to radiation therapy for head and neck cancer*. J Can Dent Assoc, 2003. **69**(9): p. 585-90.
17. Andrews, N. and C. Griffiths, *Dental complications of head and neck radiotherapy: Part 2*. Aust Dent J, 2001. **46**(3): p. 174-82.
18. Nucletron, *Oncentra Mater Plan v1.5, Physics reference manual 2006*, Nucletron B.V Veendaal The Netherlands.
19. Mackie, T.R., A.F. Bielajew, D.W. Rogers, and J.J. Battista, *Generation of photon energy deposition kernels using the EGS Monte Carlo code*. Phys Med Biol, 1988. **33**(1): p. 1-20.

20. Hurkmans, C., T. Knoos, P. Nilsson, G. Svahn-Tapper, and H. Danielsson, *Limitations of a pencil beam approach to photon dose calculations in the head and neck region*. *Radiother Oncol*, 1995. **37**(1): p. 74-80.
21. Knoos, T., C. Ceberg, L. Weber, and P. Nilsson, *The dosimetric verification of a pencil beam based treatment planning system*. *Phys Med Biol*, 1994. **39**(10): p. 1609-28.
22. Ahnesjo, A., *Collapsed cone convolution of radiant energy for photon dose calculation in heterogeneous media*. *Med Phys*, 1989. **16**(4): p. 577-92.
23. Thomas, S.J., *Relative electron density calibration of CT scanners for radiotherapy treatment planning*. *Br J Radiol*, 1999. **72**(860): p. 781-6.
24. Trapp, J.V., S.A. Back, M. Lepage, G. Michael, and C. Baldock, *An experimental study of the dose response of polymer gel dosimeters imaged with x-ray computed tomography*. *Phys Med Biol*, 2001. **46**(11): p. 2939-51.
25. Knoos, T., M. Nilsson, and L. Ahlgren, *A method for conversion of Hounsfield number to electron density and prediction of macroscopic pair production cross-sections*. *Radiother Oncol*, 1986. **5**(4): p. 337-45.
26. International Atomic Energy Agency, *Implementation of the International code of practice on dosimetry in radiotherapy (TRS 398) : review of testing results : final report of the coordinated research projects on implementation of the International code of practice TRS 398 at secondary standards dosimetry laboratories and hospitals*. IAEA-Tecdoc, 1455. 2005, Vienna: IAEA. 102.
27. Kawrakow, I., *Accurate condensed history Monte Carlo simulation of electron transport. I. EGSnrc, the new EGS4 version*. *Med Phys*, 2000. **27**(3): p. 485-98.
28. Wieslander, E. and T. Knoos, *A virtual linear accelerator for verification of treatment planning systems*. *Phys Med Biol*, 2000. **45**(10): p. 2887-96.
29. Haraldsson, P., A. Karlsson, E. Wieslander, H. Gustavsson, and S.A. Back, *Dose response evaluation of a low-density normoxic polymer gel dosimeter using MRI*. *Phys Med Biol*, 2006. **51**(4): p. 919-28.
30. NIST. Atomic composition PMMA [Web] [cited 2007-02-13]; Available from: <http://physics.nist.gov/cgi-bin/Star/compos.pl?matno=223>.
31. NIST. Atomic composition PVC. [cited 2007-02-13]; Available from: <http://physics.nist.gov/cgi-bin/Star/compos.pl?matno=232>.